

Conditional Deletion of *Eaf1* Induces Murine Prostatic Intraepithelial Neoplasia in Mice



Laura E. Pascal^{*,1}, Fei Su^{*,†,1}, Dan Wang^{*}, Junkui Ai^{*}, Qiong Song^{*,‡}, Yujuan Wang[‡], Katherine J. O'Malley^{*}, Brian Cross^{*}, Lora H. Rigatti[§], Anthony Green[¶], Rajiv Dhir[¶] and Zhou Wang^{*,¶,#,**}

^{*}Department of Urology, University of Pittsburgh School of Medicine, Pittsburgh, PA 15232, USA; [†]The Center for Metabolic and Degenerative Diseases, The Brown Foundation Institute of Molecular Medicine, University of Texas Health Science Center at Houston, Houston, TX 77030; [‡]Key Laboratory of Longevity and Aging-related Diseases of Chinese Ministry of Education, Center for Translational Medicine & School of Preclinical Medicine, Guangxi Medical University, Nanning, Guangxi 530021, China; [§]Division of Laboratory Animal Resources, University of Pittsburgh Cancer Institute, University of Pittsburgh, Pittsburgh, PA 15261, USA; [¶]Department of Pathology, University of Pittsburgh School of Medicine, Pittsburgh, PA, USA; [#]Department of Pharmacology and Chemical Biology, University of Pittsburgh School of Medicine, Pittsburgh, PA, USA; ^{**}UPMC Hillman Cancer Center, University of Pittsburgh School of Medicine, Pittsburgh, PA, USA

Abstract

ELL-associated factor 1 is a transcription elongation factor that shares significant homology and functional similarity to the androgen-responsive prostate tumor suppressor ELL-associated factor 2. EAF2 is frequently down-regulated in advanced prostate cancer and *Eaf2* deletion in the mouse induced the development of murine prostatic intraepithelial neoplasia. Here we show that similar to EAF2, EAF1 is frequently down-regulated in advanced prostate cancer. Co-downregulation of EAF1 and EAF2 occurred in 40% of clinical specimens with Gleason score >7. We developed and characterized a murine model of prostate-epithelial specific deletion of *Eaf1* in the prostate and crossed it with our previously generated mouse with conventional deletion of *Eaf2*. The prostates of *Eaf1* deletion mice displayed murine prostatic intraepithelial neoplasia lesions with increased proliferation and inflammation. Combined deletion of *Eaf1* and *Eaf2* in the murine model induced an increased incidence in mPIN lesions characterized by increased proliferation and CD3+ T cells and CD19+ B cells infiltration compared to individual deletion of either *Eaf1* or *Eaf2* in the murine prostate. These results suggest that EAF1 may play a tumor suppressive role in the prostate. Cooperation between EAF1 and EAF2 may be important for prostate maintaining prostate epithelial homeostasis, and concurrent loss of these two tumor suppressors may promote prostate tumorigenesis and progression.

Neoplasia (2019) 21, 752–764

Introduction

ELL-associated factor 1 (EAF1) was first identified based on its ability to interact with transcriptional elongation factor for RNA polymerase II (ELL) and is expressed in many tissues, including the prostate [1]. EAF1 and its functional homolog ELL-associated factor 2 (EAF2) can interact with RNA polymerase II elongation factors ELL and ELL2 proteins to facilitate binding of RNA polymerase II and control the rate of transcription elongation [2,3]. Human EAF1 and EAF2 share 58% identity and 74% amino acid sequences, and both contain a transcriptional activation domain [2]. In lower organisms, the EAF ortholog has been shown to play an important role in growth, DNA damage response, fertility, survival and development. EAF in *S. pombe* was shown to increase transcriptional elongation of spELL [4]; and deletion of spEAF inhibited growth and sensitized cells to DNA damage [5]. Deletion of *eaf-1* in *C. elegans* resulted in decreased fertility, decreased survival and altered cuticle collagen function [6]. In zebrafish, *eaf1* and *eaf2* appear to have overlapping function in modulating Wnt signaling during embryonic development [7].

In mammalian cells, there are two EAF proteins, EAF1 and EAF2 [1,2]. EAF proteins can form chimeric fusion proteins with Mixed lineage leukemia protein (MLL) resulting in the immortalization of hematopoietic progenitor cells [2]. While both EAF1 and EAF2 can bind to ELL via the amino-terminus, only EAF1 can also bind to the carboxy-terminus of ELL [2], suggesting that EAF1 and EAF2 may have unique functional interactions with the ELL proteins. EAF1 and EAF2 are required for the recruitment and retention of non-homologous end joining DNA repair proteins, and mice deficient in EAF2 were more susceptible to DNA damage [8].

In the prostate, EAF2 is up-regulated by androgens and has been shown to act as a tumor suppressor [9,10]. EAF2 down-regulation is frequent in prostate cancer, particularly in high-grade tumors [9,11,12]. EAF2 knockdown in prostate cancer cell lines induced increased proliferation, migration and invasion [13]. In murine models, deletion of *Eaf2* induced prostate intraepithelial neoplasia lesions characterized by increased proliferation and vascularization in multiple strains [10,11]. Individual knockdown of either EAF1 or EAF2 sensitized prostate cancer cells to DNA damage [8]. Since EAF1 and EAF2 have some overlapping function in mammalian cells, EAF1 may also have a role in maintaining prostate homeostasis.

Here, we compared the mRNA expression of *EAF1* in normal and prostate tumor specimens and determined the frequency of combined down-regulation of *EAF1* and *EAF2* in Gleason 6-7 compared to Gleason 8-9 tumor specimens. We determined the localization of *Eaf1* mRNA in the murine prostate and generated and characterized a murine model of prostate-specific *Eaf1* deletion. Finally, we examined the murine prostate phenotype induced by combined deletion of conditional deletion of *Eaf1* and conventional deletion of *Eaf2* to determine whether their combined loss had an additive impact on prostate homeostasis in aged animals.

Materials and Methods

Protein Sequence Comparison

The amino acid sequences used for comparison in this study were downloaded from UniProt Knowledgebase (UniProtKB) [14,15] and included: mouse *Eaf1* UniProtKB Q9D4C5, mouse *Eaf2* UniProtKB Q91ZD6, and human EAF1 UniProtKB Q96JC9. Sequence comparison was performed using the UniProt Clustal Omega

program [16] and alignment images were generated using BOXSHADE version 3.21, written by K. Hofmann and M. Baron.

In Situ Hybridization

Murine prostate tissue cryosections (ProbeOn, Fisher Biotech, Pittsburgh, PA) were washed with PBS, fixed in 4% paraformaldehyde, digested with proteinase K at 20 µg/ml in PBS, refixed in 4% paraformaldehyde, rewashed in PBS, and then acetylated in 0.25% acetic anhydride in 0.1 M triethanolamine, pH 8.0. Full-length *Eaf1* cDNA was inserted into the EcoRI and XhoI site between T3 and T7 promoters in pBluescript II SK plasmid vector. The plasmid was purified by CsCl double banding, linearized with EcoRI or XhoI, and proteinase K-treated. Purified linear DNA templates were used in the synthesis of both sense and antisense digoxigenin-labeled riboprobes using either T3 or T7 RNA polymerase (Promega Corp., Madison, WI) as previously [17,18]. Riboprobe size was reduced to approximately 250 bp using limited alkaline hydrolysis.

For hybridization, the probe was diluted in hybridization solution (5 × SSC, 1 × Denhardt's, 100 µg/ml salmon testis DNA, 50% formamide, and 250 µg/ml yeast transfer RNA), and slides were hybridized overnight at 67 °C in a sealed chamber humidified with 5 × SSC/50% formamide. Coverslips were removed, and slides were washed in 0.2 × SSC at 72 °C for 1 hour. After washing in buffer (0.1 M Tris (pH 7.6), 0.15 M NaCl), slides were blocked in 10% horse serum at room temperature for 1 hour. Slides were then incubated overnight at 4 °C with antidigoxigenin-AP Fab fragments (1:2000, Boehringer Mannheim, Mannheim, Germany) in 1% horse serum. Slides were washed and then developed with nitro blue tetrazolium (2.25 µl/ml) and 5-bromo-4-chloro-3-indolyl-phosphate, 4-toluidine salt (0.6 µg/ml) in alkaline phosphatase buffer (0.1 M Tris (pH 9.5), 0.05 M MgCl₂, 0.1 M NaCl).

Laser-Capture Microdissection and Quantitative PCR

Human prostate tumor specimens without any previous chemo-, radio- or hormone therapy were sectioned and evaluated by a board-certified genitourinary pathologist (RD). *EAF1* and *EAF2* mRNA levels were determined in specimens from 34 prostate cancer patients (19 patients with Gleason ≤7 and 15 patients with Gleason >7). Prostate cancer cells and adjacent normal glandular cells were isolated by laser-capture microdissection using a Leica LMD6000 Microsystems microscope (Wetzlar, Germany) equipped with a HV-D20P Hitachi (Tokyo, Japan) color camera and Leica Laser Microdissection V 6.3 imaging software (Wetzlar, Germany). Tissue samples were processed as described previously [19], using the Cells Direct OneStep qPCR kit from Invitrogen (Carlsbad, CA) according to manufacturer's protocol including DNase digestion step to ensure that starting material included no genomic DNA. Primers were designed to span exon junctions using PrimerBank [20] or Primer3 software (Totowa, NJ,) and optimized to within 98% to 102% efficiency. Efficiencies were incorporated into calculations for qPCR using the ΔC_p (crossing point) method ($R = 2^{[C_p \text{ sample} - C_p \text{ control}]}$) in which the relative expression ratio (R) for each sample was to GAPDH. Primers used were listed in Table 1. All assays were run on an ABI Step-One Plus thermocycler (Applied Biosystems Inc., Carlsbad, CA).

Constructs

Murine gene-targeting *Eaf1* vectors for *loxP* insertions into introns 1-2 and 2-3 of the *Eaf1* gene were generated using a bacterial artificial

chromosome (BAC) recombineering method [21] involving two major steps. First, the targeting sequence from the BAC was retrieved, a 155 K bp BAC clone (RP22-19H18) containing the entire *Eaf1* gene into locus (RP22-19H18 was screened from 129S6/SvEvtac female mouse spleen BAC clone RPCI - 22 Mouse BAC Library <http://bacpac.chori.org>) and transformed into EL350 cells. To generate a retrieval vector, homology regions for the 5' and 3' ends of the long arms of the targeting vector were joined by fusion PCR and ligated into a starting ampicillin-resistant vector (PL253, NCI-Frederick), using the restriction enzymes *NotI* and *SpeI* (New England Biolabs, Ipswich, MA, USA). A targeting sequence from the BAC DNA, a 12, 363-bp fragment containing the complete *Eaf1* genomic sequence was then retrieved into this vector using recombineering in DY380 cells, and the resultant targeting vector PL253-mEaf1 was selected using chloramphenicol and ampicillin. Second, a modified BAC containing *loxP* sites for insertion into the *Eaf1* locus was generated. A previously described *loxP*-neomycin resistance gene (Neo)-*loxP* cassette from PL452 was inserted into a cloning vector (pGEM-T Easy, Promega, Madison, WI, USA). Additional 5' and 3' short homology arms to the 3' untranslated region (UTR) of *Eaf1* were then attached to this neo cassette through an additional round of fusion PCR. This neo cassette was then inserted 283 bp upstream of the *Eaf1* exon 2 using homologous recombination using a recombineering-competent bacterial strain (EL350), resulting PL253-mEaf1-neo-L, followed by removal of Neo-*loxP* by arabinose induction of Cre recombinase [21], resulting PL253-mEaf1-LoxP-L. Similarly, another *frt*-Neo-*frt*-*loxP* cassette from pL451 was inserted 1333 bp downstream of the *Eaf1* exon 2 to

complete the final cko-targeting vector. All constructs were verified by sequencing including the 12.4 kb fragment containing the floxed *Eaf1* genomic sequence on cko-targeting vector. Primers for homology arms AB, CD, EF, GH, IJ, YZ recombination were listed in Table 1.

Generation of *Eaf1^{pc/-}* (*Eaf1^{pc/-}* (*PB-Cre4:Eaf1^{fl/fl}*) and *Eaf1^{pc/-}:Eaf2^{-/-}* Mice

The *Eaf1* cko-targeting vector was subsequently linearized with *Pvu* -*Sal* and electroporated into 129/SvEvTac by the Transgenic and Gene Targeting (TGT) Core Facility of the University of Pittsburgh; the transformants were selected for their G418 and ganciclovir (Ganc). Correctly targeted embryonic stem (ES) cell clones were identified by Southern blot and PCR analyses. The 408 bp of 5' probe and 530 bp of 3' probe for Southern blot were synthesized with mouse genomic DNA (G3091, Promega, Madison, WI, USA) using the ES-5 probe-Fw primer set and ES-3 probe primer set listed in Table 1. Genotyping of ES cell clones was performed by PCR using the *Eaf1*-L-LoxP primer set and *Eaf1*-neoR primer set listed in Table 1. Nine ES cell clones were selected for blastocyst injection, and germline transmission was established for 1 of 3 chimeric founder animals. The chimeric founder animal was then crossed to C57BL/6 J mice and germline transmission of the *loxP*-flanked *Eaf1* allele in F1 progenies was confirmed on the resulting pups by PCR with the same two sets of primers and Southern blot analysis with the same set of probes as used for ES cell selection. Offspring containing the *Eaf1^{fllox}* allele were then bred to homozygosity for this allele (*Eaf1^{fl/fl}*). *Eaf1^{fl/fl}* mice were then crossed

Table 1. Primers for PCR

HUGO* Gene Name, Application, Species	Primer ID	Sequence
ELL-associated factor 1 (EAF1), LCM-qPCR, Human	<i>EAF1</i> For	5'-ACGGCCTTACCAGAAAAGACTGTGT-3'
	<i>EAF1</i> Rev	5'-ATGTCAACTCAGCCCTCAGCTCT-3'
	<i>EAF1</i> Probe	5'-6FAM CACCCTCAGAAATGACTTGCAGTTGAG TAMRA-3'
ELL-associated factor 2 (EAF2), LCM-qPCR, Human	<i>EAF2</i> For	5'-CCAGGA CTCCCAATCTTGTA-3'
	<i>EAF2</i> Rev	5'-TAGCTTCTGCCTTCAGTTCTT-3'
	<i>EAF2</i> Probe	5'-6FAM CTCCATCTGAAGATAAGATGTCCCCAGCA TAMRA-3'
Glyceraldehyde-3-phosphate dehydrogenase (GAPDH), LCM-qPCR, Human	<i>GAPDH</i> For	5'-CATGTTTCGTCATGGGTGTGA-3'
	<i>GAPDH</i> Rev	5'-GGTGCTAAGCAGTTGGTGGT-3'
	<i>GAPDH</i> Probe	5'-6FAM ACAGCCTCAAGATCATCAGCAATGCCTC TAMRA-3'
ELL-associated factor 1 (Eaf1), Homology arms recombination, Mouse	Primer a	5'-ATAAGAATGCGGCCGCAAATCCTCTCATCGCAACC -3'
	Primer b	5'-GTCCCCAAGCTTCCGGAAACCAATCTACTCC -3'
	Primer y	5'-GTCCCCAAGCTTTTGCCCTTGTGCCAGAAC -3'
	Primer z	5'-TCTGGACTAGTGTCTGCATTCACCTCTGC -3'
	Primer c	5'-AAACGCGTCGACCTCCCTGTACTAAATGATGG -3'
	Primer d	5'-GTCCCGGAATCTCTAGACAATATTTCTGGCACTGAG -3'
	Primer e	5'-ATACGCGGATCCAGACAGAAGGATTACTGG -3'
	Primer f	5'-ATAAGAATGCGGCCGCGTACCTATGGAAAGACAGC -3'
	Primer g	5'-ATAAGTCGACAAGTGGAGAGTGATTGAGG -3'
	Primer h	5'-GTCGAATCTACTAGTAACCTGCTGTGTCTGAGG -3'
	Primer i	5'-ATAGGATCCCTGTAACCTGGTGACAGAGTGC -3'
	Primer j	5'-GTCGCGGCCGCCCTTCAGCCCCCTTAACCTGC -3'
ELL-associated factor 1 (Eaf1), ES cell clones genotyping, Southern blot, Mouse	ES-5 probe-Fw	5'-ACTTAACACTCCCAGATGC-3'
	ES-5 probe-Rev	5'-TTCTTTCAGTTTATGGGTACG-3'
	ES-3 probe-Fw	5'-CAGGAACAGAAAAGCTAGG-3'
	ES-3 probe-Rev	5'-AGGTAAGAAGAGGAAGTTGG-3'
ELL-associated factor 1 (Eaf1), ES cell clones genotyping, PCR, Mouse	<i>Eaf1</i> -L-LoxP-F1	5'-AACAGTTCCTATCTCAGTGC-3'
	<i>Eaf1</i> -L-LoxP-R1	5'-GTAATGGTGACTTCATCTCC-3'
	<i>Eaf1</i> -neoR F1	5'-GATTGGGAAGACAATAGC-3'
	<i>Eaf1</i> -neoR R1	5'-GGAGTTCAGATGAAAAGG-3'

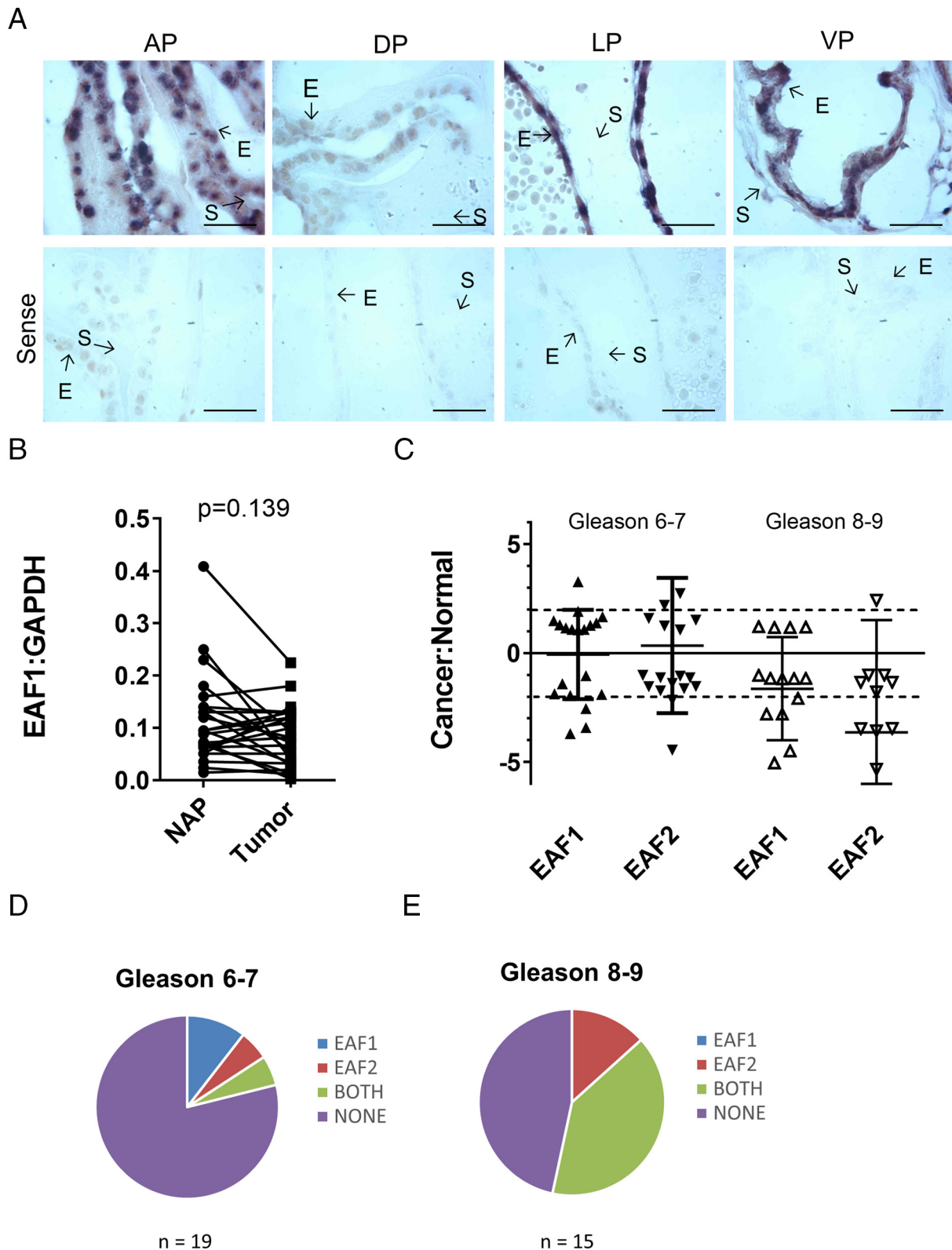


Figure 1. Expression of EAF1 in human and murine prostate. (A) In situ hybridization analysis of *Eaf1* mRNA in murine prostate tissue. Both anti-sense (upper panels) and sense (lower panels) *Eaf1* RNA probes were labeled with DIG and analyzed with alkaline phosphatase-conjugated anti-DIG antibody. Epithelial (E) and stromal (S) cells are indicated by arrows. Images are representative of results from 3 individual mice. AP, anterior prostate, DP, dorsal prostate, LP, lateral prostate, VP, ventral prostate. (B) *EAF1* mRNA expression levels in normal adjacent luminal epithelial prostate cells (NAP) and tumor cells isolated by laser-capture microdissection in treatment naïve patient tissues. (C) *EAF1* and *EAF2* mRNA expression levels in epithelial cells expressed as fold change cancer:normal. Down-regulation was defined as a decrease greater than or equal to twofold (dotted line). Each point represents one patient sample. (D) Percent of prostate cancer specimens with downregulation of *EAF1* (EAF1), downregulation of *EAF2* (EAF2), co-downregulation of *EAF1* and *EAF2* (both) or no downregulation in either *EAF1* or *EAF2* (none) in lower Gleason score (6-7) and higher Gleason score (8-9). A Fisher's exact test was used to determine whether co-downregulation was significant in high-Gleason-grade samples (6/15) compared to lower-Gleason-grade samples (1/19) ($P = .0282$).

with *ARR2Probasin-Cre* mouse (*PB-Cre4*) (kindly provided by Dr. P. Roy-Burman, University of Southern California, Los Angeles, CA, USA) [22] to generate *PB-Cre4; Eaf1^{fl/fl}* (*Eaf1^{pc/-}*) mice. The *PB-Cre4* mouse was on an B6D2F1 background which is a cross between female C57BL/6 J and male DBA/2 mice and the prostates appeared normal with no reported histological defects [22]. We then crossed the F1 *Eaf1^{pc/-}* mice with C57BL/6 J mice for a minimum of six generations to generate the *Eaf1^{pc/-}* mice on a C57BL/6 J background (Stock # 000664, Jackson Laboratory).

Eaf1^{pc/-} were then intercrossed with our previously generated conventional *Eaf2* deletion (*Eaf2^{-/-}*) mice on a C57BL/6 J background [10,11]. *Eaf1^{pc/-};Eaf2^{-/-}* mice were generated from heterozygous intercrosses of *Eaf1^{pc+/-};Eaf2^{+/-}* mice and subsequently from homozygous *Eaf1^{pc/-};Eaf2^{-/-}* intercrosses. Experimental cohorts were wild-type, *Eaf1^{pc/-}*, *Eaf2^{-/-}* and *Eaf1^{pc/-};Eaf2^{-/-}* male littermates, aged 20 to 24 months. Genotype was determined by PCR analysis of mouse-tail genomic DNA with primers listed above for *Eaf1* and as described previously for *Eaf2* [10] and *Cre* [22] lines at 21 days of age and confirmed at 20 to 24 months of age on thigh muscle genomic DNA when animals were euthanized. The urogenital tract was necropsied and samples were fixed in 10% formalin for at least 24 hours. The prostate was then microdissected from the urogenital tract, embedded in paraffin, sectioned at 4 μ m, and stained with hematoxylin and eosin (H&E) or other antibodies as described below. All mice were on a C57BL/6 background and were bred and maintained identically, under approval by the Institutional Animal Care and Use Committee of the University of Pittsburgh.

Histopathologic Analysis

H&E sections of were examined and scored by a board-certified animal pathologist in a blinded fashion (LHR, V.M.D.). Lesions were identified as epithelial hyperplasia and murine prostatic intraepithelial neoplasia (mPIN) per the criteria published by Shappell et al. commonly used to score prostate lesions in transgenic mouse models [23]. Epithelial hyperplasia was recognized as an increase in epithelial cells within normal-appearing gland profiles, reflected by stratification of epithelial cells (Shappell et al. 2004). mPIN ranged from low grade, characterized by glands lined by 1 to 3

layers of epithelial cells displaying minimal pleomorphism or hyperchromasia, slight nuclear enlargement with little atypia, infrequent mitosis, and essentially normal glandular profiles with only occasional hints of papillary epithelial proliferation to high grade, characterized by extensive intraglandular epithelial proliferation, formation of papillary or cribriform structures consisting of epithelial cells displaying significant nuclear atypia and hyperchromasia, cellular pleomorphism, and increased frequency of mitoses [23]. Inflammation was identified as the infiltration of inflammatory cells beyond lymphocytic infiltration, which was evident in both the wild type and knockout groups and is frequently observed in the C57BL/6 prostate [23].

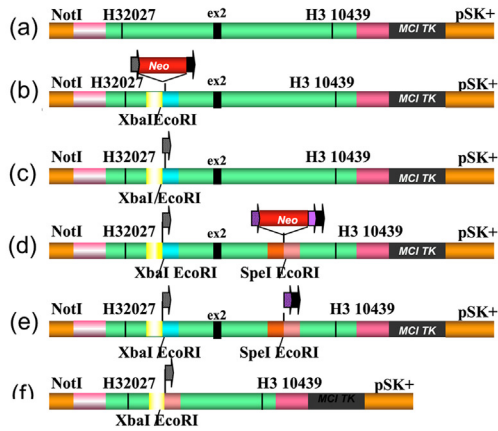
Immunohistochemistry

The slides were deparaffinized and rehydrated using a standard histology protocol. Antigen retrieval was performed using a citrate buffer (Dako, Carpinteria, CA) in Decloaking chamber at 123 °C. The slides were stained using an Autostainer Plus (Dako) platform with TBST rinse buffer (Dako). The Ki67 (D3B5) antibody (#12202, Cell Signaling Technology, Danvers, MA) and the CD3 (Rabbit Polyclonal) (CME 324, Biocare Medical, Pacheco, CA) were applied at a 1:100 dilutions. The detection used for the Ki67 and CD3 consisted of Envision + Anti-Rabbit HRP polymer (Dako). The CD19 (D4V4B) antibody (#90176, Cell Signaling Technology, Danvers, MA) was applied at a 1:800 dilution. The Rabbit Signal Stain Boost Detection Kit (Cell Signaling) was used for the detection. The substrate used for all of the above, was 3,3', diaminobenzidine (Dako). Lastly, the slides were counterstained with Hematoxylin (Cell Signaling). Immunostained sections were imaged with a Leica DM LB microscope (Leica Microsystems Inc., Bannockburn, IL) equipped with an Imaging Source NII 770 camera (The Imaging Source Europe GmbH, Bremen, Germany) and NIS-Elements Documentation v 4.6 software (Nikon Instruments, Inc., Melville, NY). All tissues were examined by a board-certified veterinary pathologist (L.H.R.) using light microscopy.

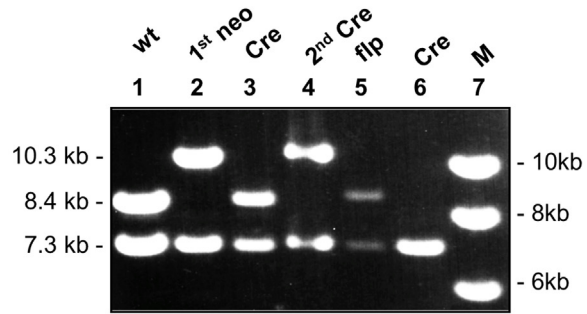
Ki-67-positive cell density was determined by analysis of sections from at least 4 independent mice from each genotype. The average number of Ki-67-positive luminal epithelial cells for each section was determined from at least 20 fields imaged at 20 \times magnification with

Figure 2. Construct an *Eaf1* exon 2 floxed allele. (A) Schematic representation of the targeting vector and the targeted allele of *Eaf1* gene. (a), the retrieving vector. (b), PL253-m *Eaf1* vector with 1st neo cassette PL253-m *Eaf1*-neo-L and (c) after neo excision PL253-m *Eaf1*-LoxP-L. (d), *Eaf1* conditional targeting vector PL253-m *Eaf1*-Neo-R. (e), the vector after FRT-based recombination PL253-m *Eaf1*-LoxP-L-R. (f), the vector after Lox P-based recombination PL253-m *Eaf1* ex2 KO. The coding exons numbered in accordance with the initiation site as exon 2 are depicted by black boxes. Green and red boxes indicate the *Eaf1* gene. The arrows denote *Lox P* or *Frt* sequence. H, Hind III site; \blacktriangle , *Lox P* sites; \blacktriangleright , *Frt* sites; ex, exon; Neo, Neomycin gene; MC1TK, TK gene; \square , *Eaf1* genomic DNA; \square , vector backbone. Region AB, light pink box, region CD and EF, yellow and turquoise boxes, region GH and region IJ, orange and pink boxes, region YZ, hot pink box. (B) *Hind III* digestion of the *Eaf1* conditional targeting vector before and after recombination in bacteria. Lanes 1 to 6 show the *Hind III* digestion patterns of the indicated vectors (a)-(f). The expected sizes of the *Hind III* restriction fragments are also indicated below the name of each vector. Lane 7 shows the size marker. (C) Schematic diagrams show the homologous recombination targeting strategy to flank the *Eaf1* coding region with *Lox P* sites, thus creating conditional *Eaf1^{fl/fl}* mice. Binding sites for Southern blot probes used to detect correctly targeted genomic DNA after restriction digestion with *Xba I* and *Spe I* are depicted. A probe for Southern blot analysis is shown as a black ellipse. Neo, neomycin-resistant gene cassette; MC1-TK, TK gene. \rightarrow , *Lox P, \rightarrow , *Frt*. (D) Southern blot analysis of genomic DNAs extracted from ES cells. *Top panel*, Southern blot with 5' probe, wide type and Flox alleles were detected as 3.9 and 3.2 kb bands after *Xba I* digestion, respectively. *Bottom panel*, Southern blot with 3' probe, wide type and Flox alleles were detected as 9.7 kb and 8.2 kb after *Spe I* digestion. (E) PCR analysis of genomic DNAs extracted from ES cells. *Top panel*, PCR analysis for L-LoxP insert, the mutant band was 280 bp; *bottom panel*, PCR analysis for R-neo cassette insert, wide type band was 394 bp and mutant band was 497 bp for R-neo cassette. C57BL/6 J was used as control.*

A

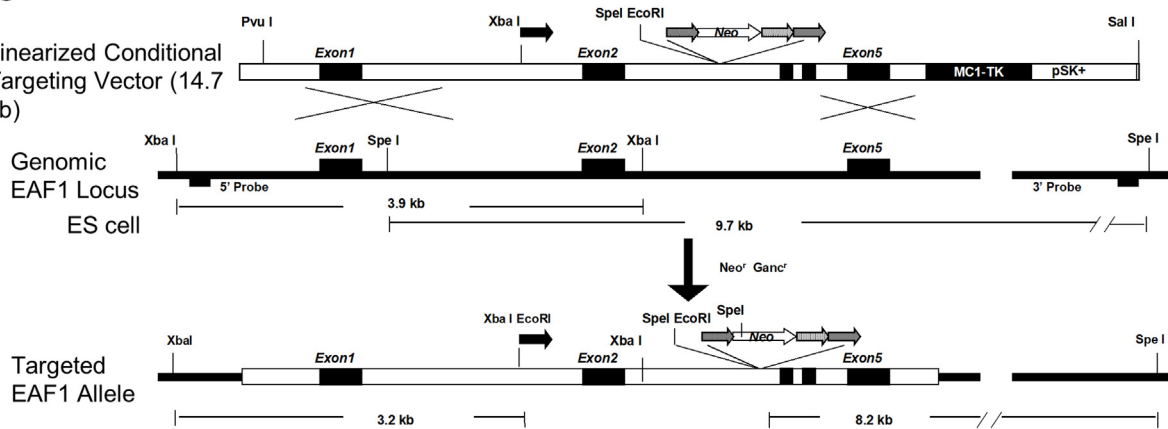


B

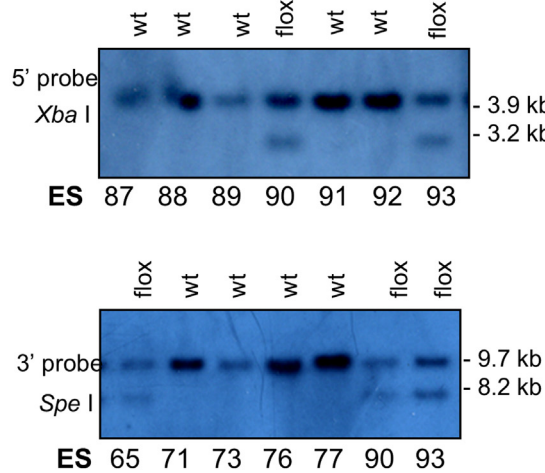


C

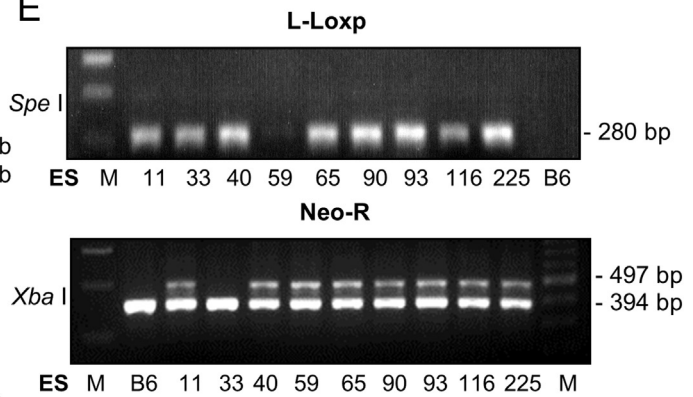
Linearized Conditional Targeting Vector (14.7 kb)



D



E



no overlap. CD3-positive cell density was determined from at least 20 fields imaged at 40 \times magnification with no overlap, CD3-positive cells within the prostate glands were counted to determine the average number of infiltrating T cells for each section. CD19-positive cell density was determined from at least 20 fields imaged at 40 \times magnification with no overlap, CD19-positive cells were counted to determine the average number of infiltrating B cells for each section.

Statistical Analysis

Comparison between groups was calculated using the Student's *t* test, the two-tailed Fisher's exact test method of summing small *P* values and the 1-way ANOVA and Bonferonni's Multiple Comparison Test as appropriate. The level of significance was set at *P* = .05. GraphPad Prism version 6 was used for graphics (GraphPad Software, San Diego, CA, USA). Values were expressed as means \pm S.D.

Results

EAF1 Protein Sequence Comparison in Mouse and Human

Sequence comparison of murine Eaf1 (UniProtKB Q9D4C5) and mouse Eaf2 (UniProtKB Q91ZD6) using UniProt [14,15] showed 52% shared identity (Supplemental Figure S1A). Comparison of murine Eaf1 with human EAF1 (UniProtKB Q9D4C5) showed a very high amino acid sequence homology, with 98% shared identity (Supplemental Figure S1B). Human EAF1 and EAF2 share 58% identity [2].

EAF1 Expression in Mouse and Human Prostate

EAF2 is expressed by epithelial cells in both the human [9] and murine prostate [11]. In situ hybridization to determine the cell type-specific expression of *Eaf1* mRNA in the murine prostate demonstrated that, similar to *Eaf2* [11], *Eaf1* expression was localized to prostate epithelial cells with no apparent expression in stromal cells (Figure 1A). Epithelial cells from normal adjacent and prostate cancer specimens were isolated by LCM and mRNA levels of EAF1 were analyzed by qPCR. Similar to the murine prostate, EAF1 mRNA expression was detected in both normal adjacent luminal epithelial cells as well as in prostate tumor cells. Overall expression levels were not differentially expressed between tumor and normal adjacent prostate (*P* = .139) (Figure 1B). Compared to normal adjacent prostate epithelial cells, EAF2 mRNA has previously been reported to be significantly down-regulated in prostate cancer specimens, particularly in high grade tumors [9,11,12]. To determine the frequency of EAF1 and EAF2 co-downregulation, EAF1 and EAF2 mRNA expression in normal adjacent and prostate cancer was determined in several specimens from prostate cancer patients and stratified according to Gleason score (Figure 1C). In prostate cancer specimens with low Gleason scores (Gleason 6-7), EAF1 down-regulation alone of twofold change or more was observed in 2/19 patients and EAF2 down-regulation alone was observed in 1/19 patients (Figure 1D). One patient displayed down-regulation of both

Table 2. Distribution of mice studied for prostatic defects.

Genotype	Number of animals analyzed	Animals with mPIN (%)	Fisher's exact <i>P</i> -value	Animals with inflammation (%)	Fisher's exact <i>P</i> -value
WT	10	0 (0%)		2 (0%)	
<i>Eaf1^{pc-/-}</i>	28	18 (64.3%)	<i>P</i> = .005	10 (35.7%)	<i>P</i> = .28
<i>Eaf2^{-/-}</i>	24	21 (87.5%)	<i>P</i> = .0001	14 (58.3%)	<i>P</i> = .032
<i>Eaf1^{pc-/-}; Eaf2^{-/-}</i>	9	9 (100%)	<i>P</i> = .0001	6 (66.7%)	<i>P</i> = .032

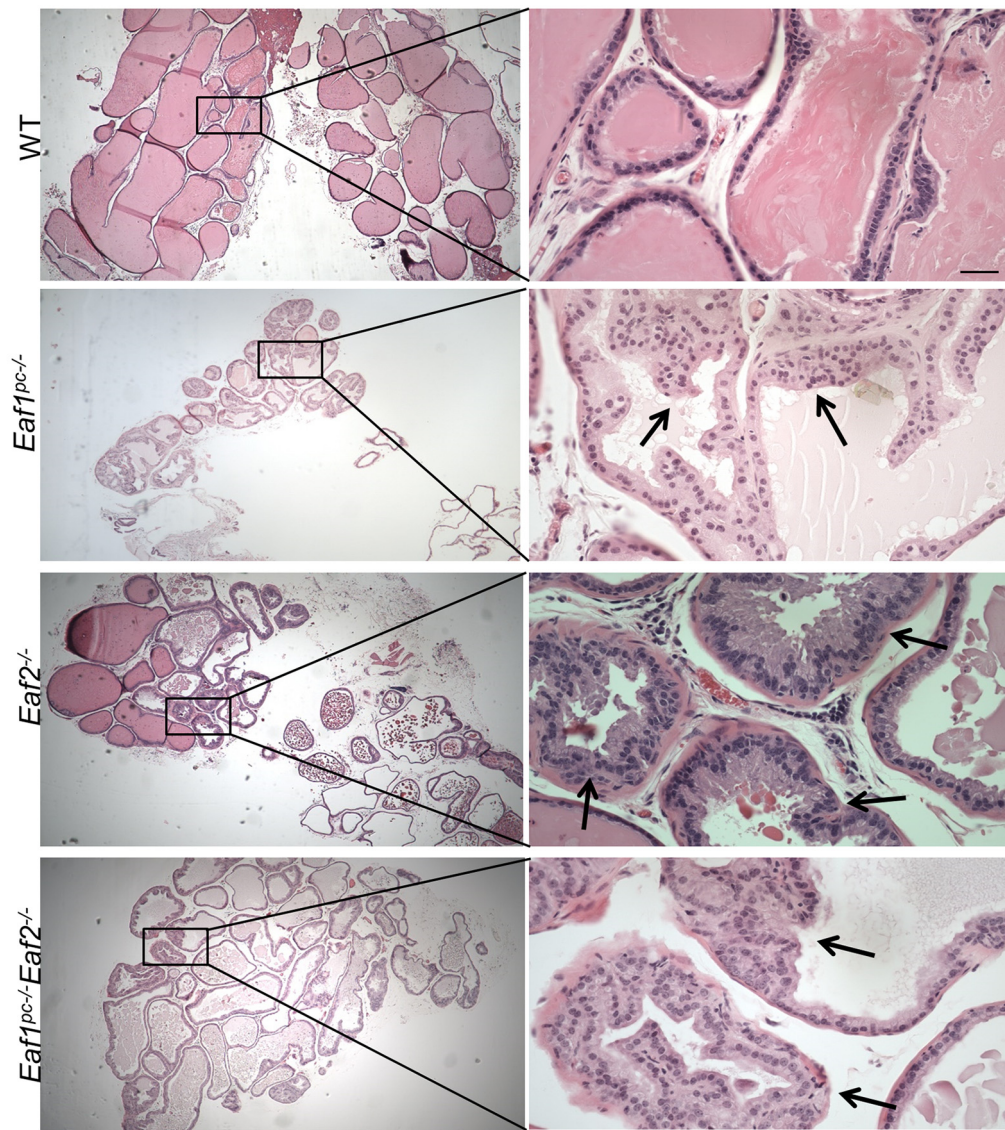
EAF1 and EAF2 in Gleason 6-7 prostate cancer, while 15/19 patients had less than 2-fold change in either EAF1 or EAF2 mRNA compared to normal adjacent tissue. In contrast, co-downregulation of EAF1 and EAF2 was detected in 6/15 prostate cancer specimens with Gleason scores 8-9, and this difference was statistically significant (*P* = .0282) (Figure 1E). These findings suggested that EAF1 and EAF2 co-downregulation was associated with aggressive prostate tumors.

Generation of Eaf1 Floxed Mice and Mice with Prostate Epithelial-Specific Deletion of Eaf1

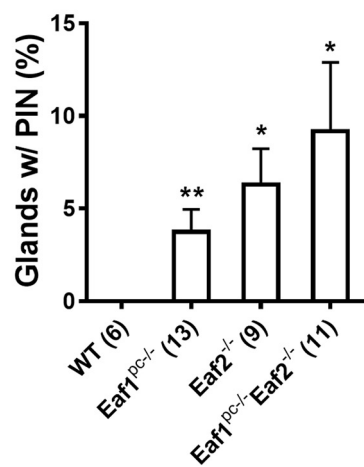
Conventional deletion of Eaf1 is embryonic lethal in the mouse [24]. Thus, we generated a conditional Eaf1-floxed (*Eaf1^{fl/fl}*) murine model crossed it with the PB-Cre4^{Tg} mouse [22] to generate prostate epithelial-specific deletion of *Eaf1*. The murine *Eaf1* gene is encoded by 6 exons that span 14.78-kb long genomic DNA. The targeting vector was designed to conditionally disrupt exon 2 using Cre-*loxP* technology [25], causing a frame-shift that would result in stop codons in all 3 reading frames. The targeted exon 2 was modified to express *Eaf1* even in the presence of a neo-resistant gene cassette in intron 2-3 and to insert *LoxP* sites flanking the single exon 2 (Figure 2A). Digestion of the retrieving vector PL253-mEaf1, first targeting vectors before and excising the neo cassette, PL253-mEaf1-neo-L and PL253-mEaf1-LoxP-L with Hind III generated the expected digestion pattern (lane 1, PL253-mEaf1, 7.3 kb and 8.4 kb; lane 2, PL253-mEaf1-neo-L, 7.3 kb and 10.3 kb; lane 3, PL253-mEaf1-LoxP-L, 7.3 kb and 8.4 kb), indicating recombination had occurred. (Figure 2B). The floxed region was 1472 bp. Homologous recombination could occur either upstream and/or downstream of the *loxP* site located 5' of *Eaf1* exon 2. Sequencing confirmed that the *Eaf1* gene sequence (about 10 kb) in the PL253-mEaf1-Neo-R targeting vector was identical to the corresponding region on the RPCI-22 (129S6SvEvTac) Mouse BAC clone (19H18), which contains the entire targeted region and the sequences of the introduced neo cassette, *LoxP* sites, and that the Frt sites were all correct. L253-mEaf1-Neo-R was transformed into bacterial strains EL250 (Flpe gene under the control of arabinose-inducible promoter, P_{BAD}) and EL350 (*Cre* gene under P_{BAD}) (kindly provided by Dr. Neal Copeland, University of Texas MD Anderson Cancer Center, Houston, TX) to induce recombination at the FRT and *LoxP* sites,

Figure 3. Histology of murine prostates. (A) H&E staining of transverse sections of prostate ventral lobes from wild-type control (WT), *Eaf1^{pc-/-}*, *Eaf2^{-/-}*, and *Eaf1^{pc-/-};
Eaf2^{-/-}* mice at age 20 to 24 months. *Eaf1^{pc-/-}*, *Eaf2^{-/-}*, and *Eaf1^{pc-/-};
Eaf2^{-/-}* mice displayed prostatic intraepithelial neoplasia (black arrows). Original magnification, 5 \times , inset 40 \times . (B) Quantification of mPIN lesions was determined as the percentage of glands with mPIN compared to the total number of glands in each mouse section. The number of mice analyzed in each group in parentheses. **P* < .05, ***P* < .01.

A



B



respectively. Functional integrity of the *LoxP* and Frt sites was tested in the PL253-mEaf1-Neo-R targeting vector (Figure 2B, lane 5 and 6).

Homologous recombinants carrying the *XbaI* loxP site were identified as was introduced along with the upstream loxP site, homologous recombinants carrying this *loxP* site (the floxed allele) will generate a 3.9-kb (wild-type) and a 3.2-kb (mutant) *XbaI* fragment using a 5' probe (Figure 2C). Since a *SpeI* site along with the selection cassette was introduced to the region downstream of exon 2, targeted clones will also have a 9.7-kb *SpeI* fragment detected by the 3' probe (Figure 2C). In one electroporation experiment, 28 out of the 200 ES colonies (14%) had the floxed-*Eaf1* allele by Southern blot and PCR analysis (Figure 2, D and E). In Southern blot for 5' probe, wild-type and Flox alleles were detected as 3.9 and 3.2 kb bands, respectively; in Southern blot for 3' probe, wild-type and Flox alleles were detected as 9.7 kb and 8.2 kb respectively (Figure 2D). In PCR analysis for L-LoxP insert the *Eaf1*-L-LoxP primer set was used. These two primers were right next to each other so no PCR product was detected for wild-type while the mutant band was 280 bp due to the introduction of L-loxP site. The *Eaf1*-neoR primer set was used in PCR analysis for the R-neo cassette insert, the wild-type band was 394 bp and mutant band was 497 bp for R-neo cassette (Figure 2E). PCR analysis and Southern blots of *Eaf1^{flox}* F1 mice tail with the indicated genotypes evidencing the germline transmission (6 out of 7) in F1 progenies (Supplemental Figure S2, A and B). Mice homozygous for the *Eaf1^{flox}* allele (referred to as *Eaf1^{fl/fl}* mice), which were expected to express intact *Eaf1*, were born healthy and fertile without any noticeable pathological phenotypes.

Selective deletion of *Eaf1* from prostate epithelium cells was performed by crossing the *Eaf1^{fl/fl}* mice with the *ARR2Probasin-Cre* mouse (*PB-Cre4^{Tg}*) (kindly provided by Dr. P. Roy-Burman, University of Southern California, Los Angeles, CA, USA) [22] to generate *PB-Cre4: Eaf1^{fl/fl}* (*Eaf1^{pc-/-}*) mice (Supplemental Figure S3A). *Eaf1^{pc-/-}* were crossed with C57BL/6 J mice for a minimum of 6 backcrosses to generate mice with a pure C57BL/6 J background. *Eaf1^{pc-/-}* then intercrossed with our previously generated conventional *Eaf2* deletion (*Eaf2^{-/-}*) mice on a C57BL/6 J background [10,11] as described in (Supplemental Figure S3B).

Eaf1 and/or *Eaf2* Deficiency Induced mPIN Lesions and Increased Proliferation in Aged Mice

Mice with conditional deletion of *Eaf1* were crossed with the *Eaf2* knockout mouse to generate wild-type *PB-Cre4^{Tg}* control (WT), *Eaf1^{pc-/-}*, *Eaf2^{-/-}*, and *Eaf1^{pc-/-}:Eaf2^{-/-}* mice. Mice in all groups were born in the expected numbers and the overall survival in all groups was not significantly different from wild-type *PB-Cre4^{Tg}* control animals (data not shown). *Eaf1^{pc-/-}* males were fertile. Grossly, the prostates of all mice displayed no visible abnormalities at age 20 to 24 months and the prostates of wild-type *PB-Cre4^{Tg}* control animals were histologically similar to wild-type C57BL/6 J mice (data not shown). Histological analysis revealed several defects in the prostates of *Eaf1^{pc-/-}* mice including the development of mPIN lesions (18/28) and stromal inflammation (10/28) (Table 2, Figure 3A). Similar to previous reports [10,11], *Eaf2* deletion induced the development of mPIN lesions (21/24) and stromal inflammation (14/24). Mice with combined deletion of *Eaf1* and *Eaf2* displayed an increased incidence in mPIN lesions (9/9) and stromal inflammation (6/9). Although there was a trend suggesting an additive effect of

combined deletion on the incidence of mPIN in *Eaf1^{pc-/-}:Eaf2^{-/-}* mice, the increased incidence was not statistically significant ($P = .079$ vs. *Eaf1^{pc-/-}*, and $P = .54$ vs. *Eaf2^{-/-}*). A subset of animals was analyzed to determine the average number of glands displaying in the ventral prostate lobes of each group. The number of glands in the ventral lobes displaying mPIN lesions was quantified as the percentage of glands with mPIN lesions compared to the total number of glands in each mouse (Figure 3B). The percentage of glands displaying mPIN lesions also displayed a trend suggesting an additive increase, however the increased incidence was also not statistically significant ($P = .197$ vs. *Eaf1^{pc-/-}*, and $P = .51$ vs. *Eaf2^{-/-}*).

The proliferative marker Ki-67 was used to detect dividing cells in the ventral prostate of each genotype. In the prostate, the number of Ki-67-positive epithelial cells was significantly increased in *Eaf1^{pc-/-}*, *Eaf2^{-/-}*, and *Eaf1^{pc-/-}:Eaf2^{-/-}* mice at age 20 to 24 months as compared to wild-type mice (Figure 4, A and B). Interestingly, the number of Ki-67-positive cells was significantly increased in *Eaf1^{pc-/-}:Eaf2^{-/-}* mice compared to mice with deletion of *Eaf1* or *Eaf2* alone suggesting an additive impact on proliferation in mice with combined deletion of *Eaf1* and *Eaf2*.

Combined Deletion of *Eaf1* and *Eaf2* Induced Inflammation in the Prostates of Aged Mice

To investigate the cooperative effects of *Eaf1* and *Eaf2* loss on the infiltration of inflammatory cells into the prostates of *Eaf1^{pc-/-}*, *Eaf2^{-/-}*, and *Eaf1^{pc-/-}:Eaf2^{-/-}* mice, we examined the number of CD3-positive T cells and CD19-positive B cells in the ventral prostates by immunostaining (Figure 5). We found that the number of CD3-positive T cells per field was significantly increased compared to wild-type controls (Figure 5, A and C). Furthermore, *Eaf1^{pc-/-}:Eaf2^{-/-}* mice had a statistically significant increase in infiltrating CD3 positive T cells compared to mice with deletion of *Eaf1* or *Eaf2* alone, suggesting an additive impact on T cell infiltration in mice with combined deletion of *Eaf1* and *Eaf2*. The number of CD19-positive B cells in the ventral prostates of *Eaf1^{pc-/-}*, *Eaf2^{-/-}*, and *Eaf1^{pc-/-}:Eaf2^{-/-}* mice was significantly higher than wild-type controls, and there was a statistically significant increase in *Eaf1^{pc-/-}:Eaf2^{-/-}* mice compared to *Eaf1^{pc-/-}* mice (Figure 5, B and D).

Discussion

The EAF proteins interact with the ELL proteins to enhance transcription elongation by suppressing transient pausing [2,3]. In the prostate, androgen-responsive EAF2 has been shown to play an important role in regulating epithelial proliferation and tumor suppression [9–12]. EAF2, and to a lesser degree, EAF1, could stabilize ELL2 and block its polyubiquitination in prostate cancer cell lines [26]. Since ELL2 has also been shown to act as a putative prostate tumor suppressor [26–28], it is likely that the interactions of EAF and ELL proteins are important for the maintenance of adult prostate homeostasis.

Here, we show that murine *Eaf1* and human EAF1 share 98% sequence identity and was expressed by epithelial cells in the murine and human prostate. EAF1 was co-down-regulated with EAF2 in advanced prostate tumor specimens, suggesting that combined loss of the EAF proteins could contribute to prostate tumor progression. *Eaf1* also appears to play a similar tumor suppressive role to *Eaf2* in the murine prostate. The prostate-

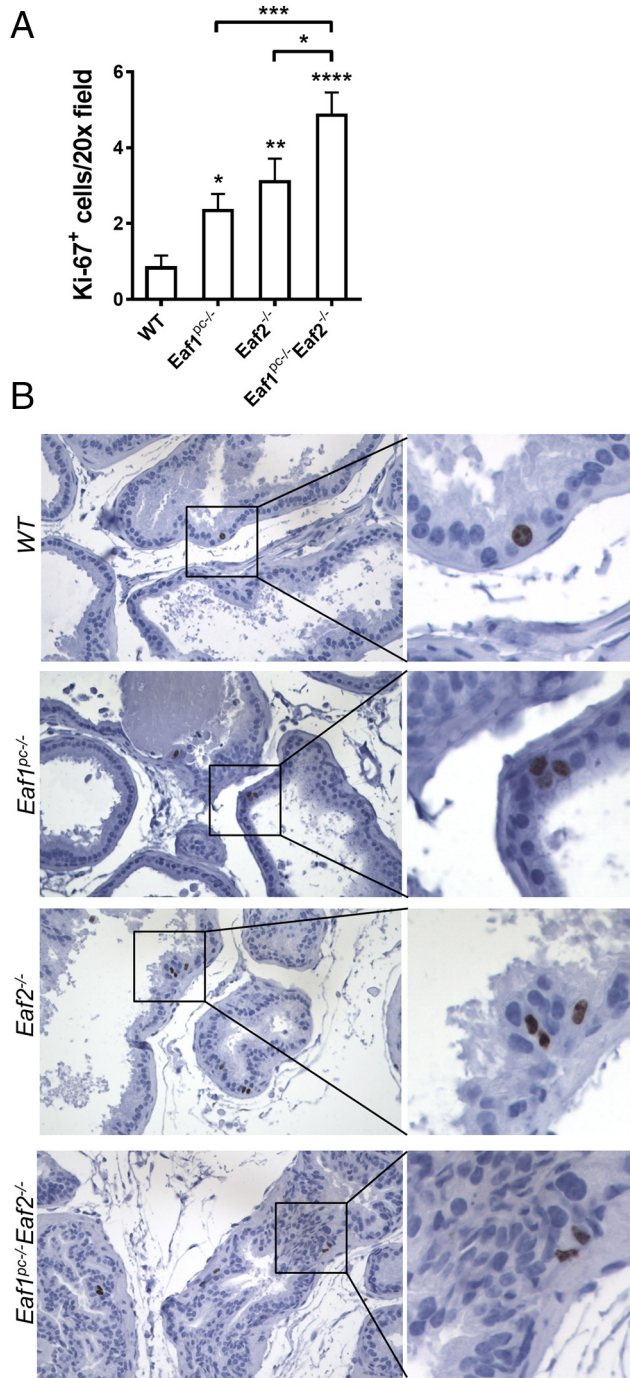


Figure 4. Effects of *Eaf1* and/or *Eaf2*-deficiency on cellular proliferation in the murine prostate. (A) Quantification of Ki-67⁺ epithelial cells in ventral prostate from wild-type control (WT), *Eaf1^{pc-/-}*, *Eaf2^{-/-}*, and *Eaf1^{pc-/-};Eaf2^{-/-}* mice at age 20 to 24 months. (B) Ki-67 immunostaining in prostate ventral lobes. Data represent average of 6 to 22 mice per group. Original magnification, 20 \times . * $P < .05$, ** $P < .01$, *** $P < .001$, **** $P < .0001$.

specific *Eaf1* knockout mouse developed mPIN lesions characterized by increased epithelial proliferation and inflammation. Combined deletion of *Eaf1* and *Eaf2* in the mouse model demonstrated an apparent additive impact on the development of mPIN lesions, proliferation and inflammation.

The development of mPIN in *Eaf1* knockout mice suggested that *Eaf1*, similar to *Eaf2*, plays a key role in maintenance of prostate homeostasis. EAF1 and EAF2 are both widely expressed in most human tissues, with minimal expression in the thymus, and share a high degree of homology and functional redundancy [1,2]. However, EAF1 is expressed in the liver and ovary while EAF2 is not, and while EAF1 can bind to the amino and carboxy terminus of ELL, EAF2 binds only to the amino-terminus of ELL and ELL2 [2]. In the mouse, *Eaf1* deletion is embryonic lethal, while *Eaf2* is not. We recently reported that *Ell2* deletion in the murine prostate could induce mPIN lesions [27] and that combined deletion of ELL2 and EAF2 phenocopied individual EAF2 or ELL2 loss in both prostate cancer cell lines and in the murine prostate [29] suggesting that EAF1 and ELL2 have overlapping function in prostate cells. In the current study, the presence of *Eaf2* was unable to prevent the development of mPIN in *Eaf1* knockout mice. Reciprocally, the presence of *Eaf1* did not prevent mPIN development in *Eaf2* knockout mice. However, combined deletion induced an apparent additive impact on the development of mPIN lesions. This observation suggests that *Eaf1* and *Eaf2* are unable to compensate for each other in maintaining prostate homeostasis. *Eaf1* and *Eaf2* may be functionally different so that one of these two closely related proteins is not able to compensate for the loss of the other. Alternatively, these two proteins may be functionally equivalent in the prostate and reduction of their expression level can lead to increased prostatic proliferation and mPIN.

The combined loss of *Eaf1* and *Eaf2* developed more mPIN lesions than knockout of either *Eaf1* or *Eaf2* alone, suggesting that loss of all of the *Eaf* family proteins is not sufficient to cause prostate cancer. Additional genetic abnormalities will be required for driving *Eaf* loss-induced mPIN lesions to prostate cancer. Our previous studies showed that PTEN heterozygosity [12] or p53 deletion [13] combined with *Eaf2* loss induced prostate cancer in mice, suggesting that down-regulation of *Eaf* family proteins is an important contributing factor for prostate carcinogenesis.

The increased infiltration of CD3-positive T-cells and CD19-positive B-cells into the *Eaf1* knockout mouse prostate is likely mediated through prostatic epithelial cell interaction with the inflammatory cells and/or changes in the prostatic microenvironment because *Eaf1* knockout was prostate epithelial cell-specific. In the case of *Eaf2* knockout mice, it is likely that the increased infiltration of CD3-positive T-cells and CD19-positive B-cells is also mediated through prostatic epithelial cell interaction with the inflammatory cells and/or change in prostatic microenvironment. Furthermore, knockdown of EAF2 in C4-2 prostate cancer cells up-regulated genes involved in inflammatory response [30]. However, *Eaf2* deletion in CD3-positive T-cells and CD19-positive B-cells may also contribute to their increased prostatic infiltration. This possibility could be addressed by generating prostate-specific *Eaf2* knockout mice.

It remains to be determined if combined deletion of *Eaf1* and *Eaf2* results in a significant increase in mPIN lesions compared to loss of *Eaf1* or *Eaf2* alone. Although there appeared to be an additive effect of combined deletion on the incidence of mPIN lesions in mice with combined deletion of *Eaf1* and *Eaf2*, we did not have enough animals to detect a significant difference in the overall incidence or the percentage of glands displaying mPIN lesions in the ventral prostates of *Eaf1^{pc-/-};Eaf2^{-/-}* mice compared to *Eaf1^{pc-/-}* ($P = .11$) or *Eaf2^{-/-}* ($P = .50$) mice. Previously, we reported that *Eaf2*

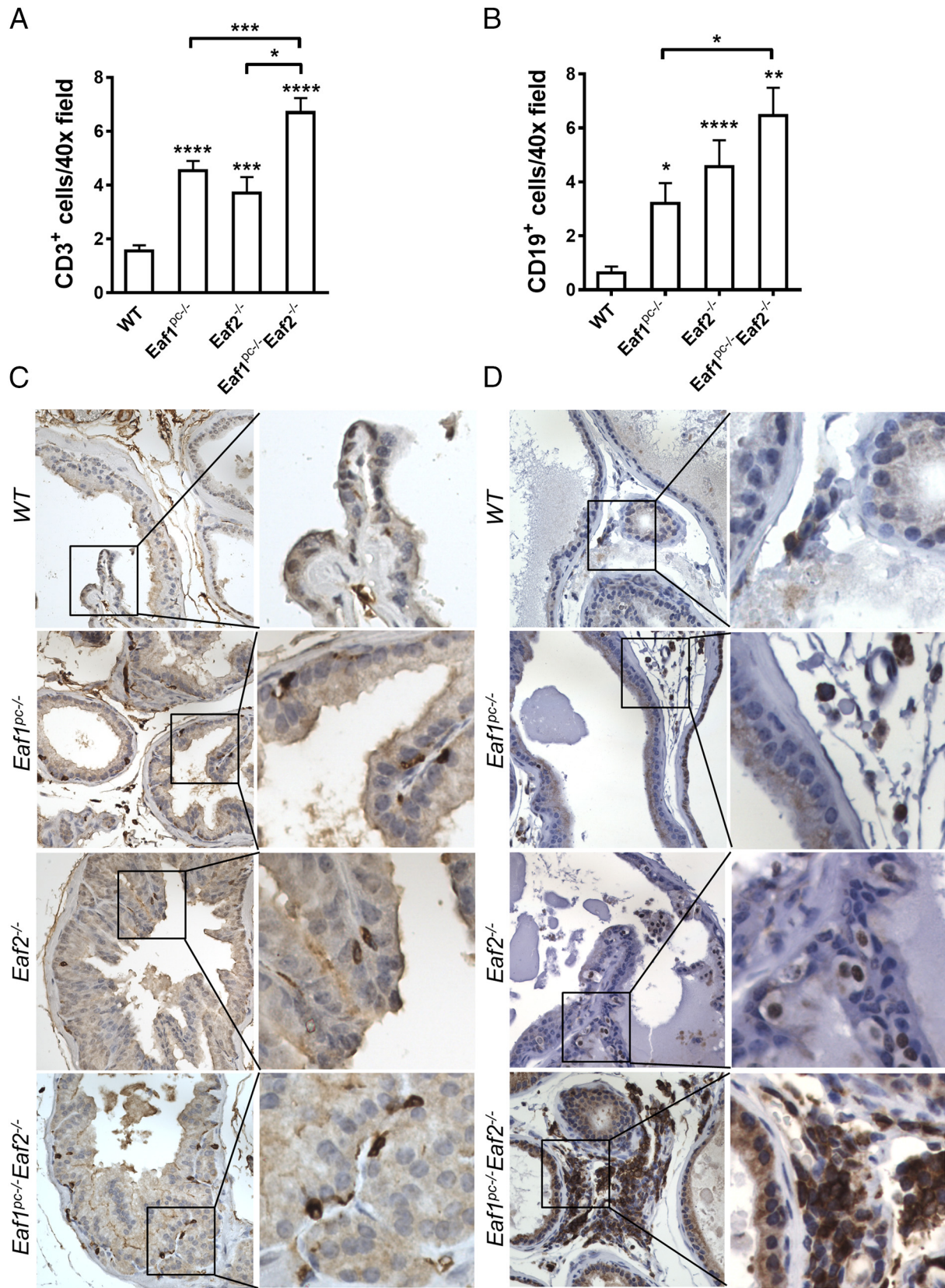


Figure 5. Effects of *Eaf1* and/or *Eaf2*-deficiency on inflammatory cells in the murine prostate. (A) Quantification of CD3⁺ T cells in ventral prostate from wild-type control (WT), *Eaf1^{pc-/-}*, *Eaf2^{-/-}*, and *Eaf1^{pc-/-}:Eaf2^{-/-}* mice at age 20 to 24 months. (B) CD3 immunostaining in transverse sections of prostate ventral lobes. (C) Quantification of CD19⁺ B cells in ventral prostate. (D) CD19 immunostaining in transverse sections of prostate ventral lobes. Data represent average of 6 to 22 mice per group. Original magnification, 40 \times . * $P < .05$, ** $P < .01$, *** $P < .001$, **** $P < .0001$.

knockout mice could develop mPIN lesions by 12 months of age [12]. In the current study, animals were not examined at younger ages to determine whether mPIN lesions developed earlier in *Eaf1^{pc} Eaf2^{-/-}* mice than in mice with *Eaf1* or *Eaf2* deletion alone. The current study was designed to determine if combined deletion of *Eaf1* and *Eaf2* was sufficient to drive prostate tumorigenesis in the murine model. Future studies examining animals at earlier time points will be required to fully elucidate the combined impact of *Eaf1* and *Eaf2* deletion on the development of pre-neoplastic lesions in the mouse prostate.

Cumulatively, these results suggest that loss of *Eaf1* murine prostate can induce pre-neoplastic PIN lesions. Combined deletion of *Eaf1* and *Eaf2* could induce a significant increase in proliferation and inflammation compared to loss of *Eaf1* or *Eaf2* alone in the murine prostate, but loss of both the Eaf proteins was insufficient to induce prostate cancer in the murine model. EAF1 and EAF2 may both act as prostate tumor suppressors and their combined down-regulation is frequent in aggressive prostate tumors.

Supplementary data to this article can be found online at <https://doi.org/10.1016/j.neo.2019.05.005>.

Competing Interests

The authors indicate no potential conflicts of interest.

Authors' Contributions

LEP performed experiments, data analysis and interpretation, and wrote the manuscript. FS performed experiments generating *Eaf1* floxed mice and helped write the manuscript. DW, JA, YW, QS, KJO and BC performed experiments. LHR provided murine prostate pathology analyses. AG performed immunostaining, RD provided human prostate tissue specimens and pathology analyses. ZW conceived and directed the study and helped write the manuscript. All authors read and approved the final manuscript.

Acknowledgements

We are grateful to Aiyuan Zhang, Katie Leschak, Robin Frederick and Megan Lambert for technical support. This work was supported in part by NIH R01 CA186780 (ZW), R50 CA211242 (LEP). This project used the UPCI Pitt Biospecimen Core and the Animal Facility and was supported in part by award P30CA047904.

References

- [1] Simone F, Polak PE, Kaberlein JJ, Luo RT, Levitan DA, and Thirman MJ (2001). EAF1, a novel ELL-associated factor that is delocalized by expression of the MLL-ELL fusion protein. *Blood* **98**, 201–209.
- [2] Simone F, Luo RT, Polak PE, Kaberlein JJ, and Thirman MJ (2003). ELL-associated factor 2 (EAF2), a functional homolog of EAF1 with alternative ELL binding properties. *Blood* **101**, 2355–2362.
- [3] Kong SE, Banks CA, Shilatifard A, Conaway JW, and Conaway RC (2005). ELL-associated factors 1 and 2 are positive regulators of RNA polymerase II elongation factor ELL. *Proc Natl Acad Sci U S A* **102**, 10094–10098.
- [4] Banks CA, Kong SE, Spahr H, Florens L, Martin-Brown S, Washburn MP, Conaway JW, Mushegian A, and Conaway RC (2007). Identification and characterization of a *Schizosaccharomyces pombe* RNA polymerase II elongation factor with similarity to the metazoan transcription factor ELL. *J Biol Chem* **282**, 5761–5769.
- [5] Dabas P, Sweta K, Ekka M, and Sharma N (2018). Structure function characterization of the ELL associated factor (EAF) from *Schizosaccharomyces pombe*. *Gene* **641**, 117–128.
- [6] Cai L, Phong BL, Fisher AL, and Wang Z (2011). Regulation of fertility, survival, and cuticle collagen function by the *Caenorhabditis elegans* eaf-1 and ell-1 genes. *J Biol Chem* **286**, 35915–35921.
- [7] Liu JX, Xu QH, Yu X, Zhang T, Xie X, and Ouyang G (2018). Eaf1 and Eaf2 mediate zebrafish dorsal-ventral axis patterning via suppressing Wnt/beta-catenin activity. *Int J Biol Sci* **14**, 705–716.
- [8] Ai J, Pascal LE, Wei L, Zang Y, Zhou Y, Yu X, Gong Y, Nakajima S, Nelson JB, and Levine AS, et al (2017). EAF2 regulates DNA repair through Ku70/Ku80 in the prostate. *Oncogene* **36**, 2054–2065.
- [9] Xiao W, Zhang Q, Jiang F, Pins M, Kozlowski JM, and Wang Z (2003). Suppression of prostate tumor growth by U19, a novel testosterone-regulated apoptosis inducer. *Cancer Res* **63**, 4698–4704.
- [10] Xiao W, Zhang Q, Habermacher G, Yang X, Zhang AY, Cai X, Hahn J, Liu J, Pins M, and Doglio L, et al (2008). U19/Eaf2 knockout causes lung adenocarcinoma, B-cell lymphoma, hepatocellular carcinoma and prostatic intraepithelial neoplasia. *Oncogene* **27**, 1536–1544.
- [11] Pascal LE, Ai J, Masoodi KZ, Wang Y, Wang D, Eisermann K, Rigatti LH, O'Malley KJ, Ma HM, and Wang X, et al (2013). Development of a reactive stroma associated with prostatic intraepithelial neoplasia in EAF2 deficient mice. *PLoS One* **8**e79542.
- [12] Ai J, Pascal LE, O'Malley KJ, Dar JA, Isharwal S, Qiao Z, Ren B, Rigatti LH, Dhir R, and Xiao W, et al (2014). Concomitant loss of EAF2/U19 and Pten synergistically promotes prostate carcinogenesis in the mouse model. *Oncogene* **33**, 2286–2294.
- [13] Wang Y, Pascal LE, Zhong M, Ai J, Wang D, Jing Y, Pilch J, Song Q, Rigatti LH, and Graham LE, et al (2017). Combined loss of EAF2 and p53 induces prostate carcinogenesis in male mice. *Endocrinology* **158**, 4189–4205.
- [14] Pundir S, Martin MJ, and O'Donovan C (2017). UniProt Protein Knowledgebase Methods Mol Biol **1558**, 41–55.
- [15] UniProt: the universal protein knowledgebase. *Nucleic Acids Res* 2017; **45**: D158–D169.
- [16] Pundir S, Martin MJ, and Tools O'Donovan C UniProt (2016). *Curr Protoc Bioinformatics* **53**, 1 29 21–15.
- [17] Cyriac J, Haleem R, Cai X, and Wang Z (2002). Androgen regulation of spermidine synthase expression in the rat prostate. *Prostate* **50**, 252–261.
- [18] Furlow JD, Berry DL, Wang Z, and Brown DD (1997). A set of novel tadpole specific genes expressed only in the epidermis are down-regulated by thyroid hormone during *Xenopus laevis* metamorphosis. *Dev Biol* **182**, 284–298.
- [19] O'Malley KJ, Dhir R, Nelson JB, Bost J, Lin Y, and Wang Z (2009). The expression of androgen-responsive genes is up-regulated in the epithelia of benign prostatic hyperplasia. *Prostate* **69**, 1716–1723.
- [20] Spandidos A, Wang X, Wang H, and Seed B (2010). PrimerBank: a resource of human and mouse PCR primer pairs for gene expression detection and quantification. *Nucleic Acids Res* **38**, D792–D799.
- [21] Liu P, Jenkins NA, and Copeland NG (2003). A highly efficient recombineering-based method for generating conditional knockout mutations. *Genome Res* **13**, 476–484.
- [22] Wu X, Wu J, Huang J, Powell WC, Zhang J, Matusik RJ, Sangiorgi FO, Maxson RE, Sucof HM, and Roy-Burman P (2001). Generation of a prostate epithelial cell-specific Cre transgenic mouse model for tissue-specific gene ablation. *Mech Dev* **101**, 61–69.
- [23] Shappell SB, Thomas GV, Roberts RL, Herbert R, Ittmann MM, Rubin MA, Humphrey PA, Sundberg JP, Rozengurt N, and Barrios R, et al (2004). Prostate pathology of genetically engineered mice: definitions and classification. The consensus report from the Bar Harbor meeting of the Mouse Models of Human Cancer Consortium Prostate Pathology Committee. *Cancer Res* **64**, 2270–2305.
- [24] Dickinson ME, Flenniken AM, Ji X, Teboul L, Wong MD, White JK, Meehan TF, Weninger WJ, Westerberg H, and Adissu H, et al (2016). High-throughput discovery of novel developmental phenotypes. *Nature* **537**, 508–514.
- [25] Abremski K and Hoess R (1984). Bacteriophage P1 site-specific recombination. Purification and properties of the Cre recombinase protein. *J Biol Chem* **259**, 1509–1514.
- [26] Yang T, Jing Y, Dong J, Yu X, Zhong M, Pascal LE, Wang D, Zhang Z, Qiao B, and Wang Z (2018). Regulation of ELL2 stability and polyubiquitination by EAF2 in prostate cancer cells. *Prostate* **78**, 1201–1212.
- [27] Pascal LE, Masoodi KZ, Liu J, Qiu X, Song Q, Wang Y, Zang Y, Yang T, Rigatti LH, and Chandran U, et al (2017). Conditional deletion of ELL2 induces murine prostate intraepithelial neoplasia. *J Endocrinol* **235**, 123–136.

- [28] Qiu X, Pascal LE, Song Q, Zang Y, Ai J, O'Malley KJ, Nelson JB, and Wang Z (2017). Physical and functional interactions between ELL2 and RB in the suppression of prostate cancer cell proliferation, migration, and invasion. *Neoplasia* **19**, 207–215.
- [29] Zhong M, Pascal LE, Cheng E, Masoodi KZ, Chen W, Green A, Cross BW, Parrinello E, Rigatti LH, and Wang Z (2018). Concurrent EAF2 and ELL2 loss phenocopies individual EAF2 or ELL2 loss in prostate cancer cells and murine prostate. *Am J Clin Exp Urol* **6**, 234–244.
- [30] Pascal LE, Wang Y, Zhong M, Wang D, Chakka AB, Yang Z, Li F, Song Q, Rigatti LH, and Chaparala S, et al (2018). EAF2 and p53 co-regulate STAT3 activation in prostate cancer. *Neoplasia* **20**, 351–363.